International Journal of Modern Physics B
Vol. 35, No. 19 (2021) 2150199 (21 pages)

DOI: 10.1142/S021797922150199X

World Scientific
www.worldscientific.com

Bio-convective couple stress nanofluid behavior analysis with temperature-dependent viscosity and higher order slip encountered by a moving surface

Yun-Xiang Li
College of Science, Hunan City University, Yiyang 413000, P. R. China

Sami Ullah Khan
Department of Mathematics, COMSATS University Islamabad, Sahiwal 57000, Pakistan

Faqir Shah
Department of Mathematics, Karakoram International University, 15100 Gilgit, Pakistan

Hassan Waqas
Department of Mathematics, Government College University Faisalabad, 31200, Layyah Campus, Pakistan

M. Ijaz Khan*
Department of Mathematics and Statistics, Riphah International University I-14, Islamabad 44000, Pakistan
Nonlinear Analysis and Applied Mathematics (NAAM) Research Group, Department of Mathematics, Faculty of Science, King Abdulaziz University, P. O. Box 80257, Jeddah 21589, Saudi Arabia
mikhan@math.qau.edu.pk

M. Y. Malik
Department of Mathematics, College of Sciences, King Khalid University, Abha 61413, Kingdom of Saudi Arabia

Received 16 April 2021
Revised 1 June 2021
Accepted 2 June 2021
Published 14 July 2021

In nanotechnology, the nanofluids are decomposition of base materials and nanoparticles where the nanoparticles are immersed in base liquid. The utilization of such

*Corresponding author.

nanoparticles into base liquids can significantly enhance the thermal features of resulting materials which involve applications in various industrial and technological processes. While studying the rheological features of non-Newtonian fluids, the constant viscosity assumptions are followed in many investigations. However, by considering the viscosity as a temperature-dependent is quite useful to improve the heating processes along with nanoparticles. Keeping such motivations in mind, this investigation reports the temperature-dependent viscosity and variable heat-dependent conductivity in bioconvection flow of couple stress nanoparticles encountered by a moving surface. The famous Reynolds exponential viscosity model is used to deploy the relations for temperature-dependent viscosity. Moreover, the activation energy and higher order slip (Wu's slip) are also elaborated to make this investigation more novel and unique. The emerging flow equations for governing flow problem are formulated which are altered into non-dimensional forms. The numerical simulations with applications of Runge–Kutta fourth–order algorithm are focused to obtain the desired solution. Before analyzing the significant physical features of various parameters, the confirmation of solution is done by comparing the results with already reported investigations as limiting cases. The results are graphically elaborated with relevant physical consequences. Various plots for velocity, temperature, concentration, wall shear stress, local Nusselt number, local Sherwood number and motile density numbers are prepared.

Keywords: Couple stress nanofluid; slip effects; nonlinear thermal radiation; temperature-dependent viscosity; numerical scheme.

PACS numbers: 47.10−g, 47.10.ab

1. Introduction

Nanotechnology is regarded by several to be one of the essential factors driving this century's new major manufacturing revaluation. It is the most important technical cutting edge still being investigated. Nanofluid thermal conductivity is an advanced technique that can be used to improve heat transformation. As a result of their applications in various fields such as natural energy, nuclear plants, polymer processing, generator technology, furnace technology, cooling gas, glass manufacturing and advanced technology, respectively. Fluid dynamics scientists have shown a strong interest in the study of base nanoliquid over the last few centuries. It allowed both liquid and nanometer-sized materials to be combined in order to increase the heat transforming ability of liquids. In order to resolve this weakness, radiant scientists develop the liquids described above by introducing a single kind of nanoparticles to form a solution labeled "nanofluid" which was first reported by Choi and Eastman.[1] Researchers have shown that nanomaterials have impressive potential to increase the rate of heat transformed and heat capacity of base liquids. Buongiorno[2] investigated the convective boundary layer movement application of the nanoliquid. Waini *et al.*,[3] studied the importance of transpiration over hybrid nanoliquid flowing and heat transformation via stretched/shrinking surface for standardized shear flow. Lund *et al.*,[4] researched the double solutions including stability study of a hybrid nanoliquid against a stretched/decreasing layer performing MHD flow. Kumar and Srinivas[5] reported the deals with the unstable hydromagnetic movement of Eyring–Powell nanoliquid across a tilted permeable

stretched sheet. Abdal *et al.*,[6] scrutinized the multi-slip influences upon its mixed convection Magnetohydrodynamic unstable movement of micropolar nanoliquids across an extending/shrinking surface together with radiation in the absence of a heat exchanger. Gireesha *et al.*,[7] investigated the impact of distance and heat-dependent energy production/absorption, thermal radiation over 3D MHD Jeffrey flow of liquids across a nonlinearly permeable stretched sheet in the absence of a porous channel. Khan *et al.*,[8] represented the performance to determine the properties of energy transformed and skin friction for 2D unsubtle stagnation point flowing of nanoliquid-dependent SWCNTs and MWCNTs across a curved surface. Hayat *et al.*,[9] discovered the Darcy–Forchheimer's two-dimensional (2D) nanoliquid flow owing to the bent stretched layer. Khan *et al.*,[10] explored the consequence of several slips on the Jeffrey liquid model of an unstable Magnetohydrodynamic viscoelastic bouncy nanoliquid in the absence of Soret and radiation throughout a permeable stretched surface. Many investigators have been interested in the research of nanofluid, see Refs. 11–16.

We also experience multiple mechanisms in nature and manufacturing companies that often see transportation systems due to variations in concentration. In the case of liquid dynamics, a chemical process occurs when the base liquid particles communicate with nanomaterials substances. The rate of the reaction and concentrations has a significant relationship during the first-order. It is necessary to discuss its influence, since the rate of mass transport in the flowing can be affected by the existence of chemical processes. In order to react spontaneously, the reactants must have a minimum amount of energy. This specified minimum amount of energy can be defined as activation energy. Arrhenius equation is utilized to calculate the activation energy for chemical processes, and it also defines the improvement in the steady rate at different temperatures. First, Bestman[17] proposed the natural mixed convection flow of binary agglomeration into a porous space through activation energy. Waqas *et al.*,[18] outlined the Numerical solution for nonlinear Radiative Eyring–Powell nanoliquid assuming magnetic dipoles as well as activation energy. Hayat *et al.*,[19] presented the effect of binary chemical processes and activation energy in third-grade nanoliquid Magnetohydrodynamic flow connected within convective situations. Sandhya *et al.*,[20] examined the impact of second-order slip or activation energy (AE) over hydromagnetic and Radiative liquid dynamics through an exponentially stretched sheet. Khan *et al.*,[21] worked on titanium oxide and graphene oxide nanoparticles in entropy optimized flow with second-order velocity slip. Ullah *et al.*,[22] explored operates with the 3D rotary motion of nanoparticles in the form of activation energy and nonlinear thermal radiation contained in the non-Darcian porous channel. Khan *et al.*,[23] identified the Arrhenius activation energy or simultaneous chemical processes are considered when assessing hydromagnetic mixed convection second-grade nanoliquid flowing across a porous medium in the absence of thermal energy, buoyancy as well as entropy production. The magneto-mixed natural convection of Eyring–Powell nanoliquid toward

the stretching sheet; the activation energy effect is discussed by Naz *et al.*[24] Khan *et al.*,[25] discussed the properties of fluid parameters such as magnetic parameter, radiation parameter, diffusion variable, Weissenberg number as well as temperature ratio parameter and nanoparticles concentration parameters for entropy generation throughout the reactionary dissipative movement of the Carreau–Yasuda liquid past the stretching sheet.

The macroscopic convection movement of nanoliquid produced by density gradient developed by the collaborative swimming microorganisms is defined as the bioconvection phenomenon. Such microorganisms are haphazard and actively swim above in the host liquid with the aid of some inspiration (chemical materials, gravitation, respectively. Gyrotactic motile microorganisms are utilized in the process of agricultural production and preservation. They have wide range medical applications in biochemistry as well as biotechnology. Bioconvection observations are utilized for the oil and gas manufacturing to improve the oil recovery methodology to raise the recovery of oil. In addition, the bioconvection of nanomaterials is connected with the concentration of stratification including the method of development owing to the interaction involving microorganisms, buoyancy forces as well as nanomaterials. It is also identified that the suspended stabilization of nanoparticles in the absence of gyrotactic motile microorganisms has been successfully improved. The definition of bioconvection was first time proposed by Platt[26] in 1961, which identified the development of cells induced through microorganisms in aqueous solution; he noted a similar nature to Rayleigh–Benard thermal conduction, where the source originated from the boundary warming structure. The energy and mass transformation of the unstable two-dimensional movement of the bioconvective non-Newtonian fluid like Maxwell nanofluid through the exponentially stretched layer is introduced by Khan and Nadeem.[27] Mondal and Pal[28] examined bioconvection flow of nanoliquid consisting microorganisms across a nonlinear expanding layer in the absence of thermal radiation, chemical processes and internal heat sources. The magnetic magnetohydrodynamics (MHD) bioconvection movements of nanofluid via stretching surface through Velocity slip or viscous dissipation are discussed by Ayodeji *et al.*[29] Khan *et al.*,[30] examined Al2O3-47 nm and Al2O3 nm hybrid nanoparticles impact in peristaltic flow in a symmetric porous channel. Ferdows *et al.*,[31] determined the MHD flow of nanofluid, containing motile microorganisms, across an exponentially rotating sheet. Khan *et al.*,[32] discussed bio-convective nanofluid flow of Sutterby fluid over a rotating disk. The unstable stagnation point movement and thermal conductivity of nanoliquid involving motile microorganisms has been reported past the permeable rotating surface by Basir *et al.*[33] Magagula *et al.*,[34] analyzed the interpretation of double-dispensed is dependent on bioconvection of the Casson nanofluid flow across a stretched surface.

This investigation corresponds too many real-world implementations such as heating development, cool organism and biomedical. The main aim of this perusal is to examine the incompressible, nonlinear radiative flow of couple stress nanofluid containing swimming microorganisms through uniformly moving surface. The

effects of temperature-dependent viscosity and activation energy are also scrutinized. The numerical outcomes are obtained through famous shooting algorithm.

2. Flow Model

After successfully illustrating the motivation of this work, this section aims to model the flow problem with governing equations. We assume an incompressible flow of couple stress nanofluid with gyrotactic microorganisms. The uniformly moving surface induced the flow. The motivated flow model is followed by using Cartesian systems while velocity components u and v are attributed in x and y directions, respectively. The nanoparticles are assumed to be magnetized due to magnetic force influence which is taken in perpendicular direction. Let T, C and N symbolize, respectively, the temperature, nanoparticles concentration and microorganism's density. The free stream nanoparticles temperature is T_∞, concentration denoted by C_∞ and microorganism's density is N_∞. With these assumptions, following system of expressions is developed for current flow problem[33,34]:

$$\frac{\partial u}{\partial x} + \frac{\partial v}{\partial y} = 0, \tag{1}$$

$$\rho\left(u\frac{\partial u}{\partial x} + v\frac{\partial u}{\partial y}\right) = \frac{\partial}{\partial y}\left(\mu(T)\frac{\partial u}{\partial y}\right) - \eta^*\frac{\partial^4 u}{\partial y^4} - \sigma^* B_0^2 u + \begin{bmatrix} (1-C_\infty)\rho_f\beta^* g(T-T_\infty) \\ -(\rho_p-\rho_f)g(C-C_\infty) - (n-n_\infty)g\gamma^*(\rho_m-\rho_f) \end{bmatrix}, \tag{2}$$

$$u\frac{\partial T}{\partial x} + v\frac{\partial T}{\partial y} = \frac{1}{(\rho c_p)_f}\frac{\partial}{\partial y}\left(k(T)\frac{\partial T}{\partial y}\right) + \frac{(\rho c_p)_p}{(\rho c_p)_f}\left\{D_B\frac{\partial T}{\partial y}\frac{\partial C}{\partial y} + \frac{D_T}{T_\infty}\left(\frac{\partial T}{\partial y}\right)^2\right\} + \frac{Q_0}{(\rho c_p)_f}(T-T_\infty) + \frac{\partial}{\partial y}\left(\frac{16\sigma^{**}}{3k^*}T^3\frac{\partial T}{\partial y}\right), \tag{3}$$

$$u\frac{\partial C}{\partial x} + v\frac{\partial C}{\partial y} = D_B\frac{\partial^2 C}{\partial y^2} + \frac{D_T}{T_\infty}\frac{\partial^2 T}{\partial y^2} - K_1 r^2\,(C-C_\infty)\left(\frac{T}{T_\infty}\right)^2 \exp\left(\frac{-E_a}{\kappa T}\right), \tag{4}$$

$$u\frac{\partial n}{\partial x} + v\frac{\partial n}{\partial y} + \frac{bW_c}{(C_w-C_\infty)}\left[\frac{\partial}{\partial y}\left(n\frac{\partial C}{\partial y}\right)\right] = D_m\left(\frac{\partial^2 n}{\partial y^2}\right). \tag{5}$$

The physical expressions associated with the above relations are temperature-dependent viscosity ($\mu(T)$), couple stress constant (η^*), magnetic field strength (B_0), electrical conductivity (σ_e), (ν), gravity (g), source coefficient, source (Q_0), kinematic viscosity volume suspension coefficient (β^*), (n) the microorganisms, density of motile microorganism particles (ρ_m), nanoparticles density (ρ_p), diffusion constant (D_B), microorganisms diffusion constant (D_m), Boltzmann constant κ, chemotaxis constant (b) and swimming cells speed W_e, k^* the mean absorption coefficient, rate constant (n), E_a is activation energy, reaction rate ($K_1 r$) and Stefan Boltzmann constant σ^{**}.

The following boundary constraints are modeled to the present flow problem

$$u = u_w + u_{\text{slip}}, \quad v = 0, \quad \frac{\partial^2 u}{\partial y^2} = 0,$$
$$-k\frac{\partial T}{\partial y} = h_f(T_f - T), \quad D_B\frac{\partial C}{\partial y} + \frac{D_T}{T_\infty}\frac{\partial T}{\partial y} = 0, \quad n = n_w, \text{ at } y = 0, \tag{6}$$

$$u \to 0, \quad \frac{\partial u}{\partial y} \to 0, \quad v \to 0, \quad T \to T_\infty,$$
$$C \to C_\infty, \quad n \to n_\infty \text{ at } y \to \infty, \tag{7}$$

where T_f expressed the convective nanoparticles temperature and h_f being heat transfer coefficient. The third boundary condition ($\frac{\partial^2 u}{\partial y^2} = 0$) attributed the vanish assumption of couple stresses at surface. The boundary conditions for slip flow are suggested via following relations:

$$u_{\text{slip}} = \frac{2}{3}\left(\frac{3 - \Gamma^* l^2}{\Gamma^*} - \frac{3}{2}\frac{1 - l^2}{k_n}\right)\varepsilon^*\frac{\partial u}{\partial y} - \frac{1}{4}\left[l^4 + \frac{2}{k_n^2}(1 - l^2)\right]\varepsilon^{*2}\frac{\partial^2 u}{\partial y^2}, \tag{8}$$

$$u_{\text{slip}} = A\frac{\partial u}{\partial x} + G\frac{\partial^2 u}{\partial x^2}, \tag{9}$$

where k_n is Knudsen number, Γ^* the coefficient of momentum and ε is symbolized for molecular mean free path.

The dimensionless form is achieved via utilization of following variables:

$$\zeta = \sqrt{\frac{a}{\nu}}y, \quad u = cxf'(\zeta), \quad v = -\sqrt{c\nu}f(\zeta),$$
$$\theta(\zeta) = \frac{T - T_\infty}{T_w - T_\infty}, \quad \varphi(\zeta) = \frac{C - C_\infty}{C_\infty}, \quad \chi(\zeta) = \frac{n - n_\infty}{n_w - n_\infty}. \tag{10}$$

The following Reynolds number exponential relations are employed to determine the relations for temperature-dependent viscosity

$$\mu(\theta) = e^{-(\gamma\theta)} = 1 - (\gamma\theta) + O(\gamma^2), \tag{11}$$

where γ is viscosity parameter.

In view of (10) and (11), the following set of non-dimensional equations is achieved

$$(1 - (\gamma\theta))f''' - \gamma\theta' f'' - (f')^2 + ff'' - Mf' - Kf'''' + \lambda(\theta - \text{Nr}\phi - \text{Nc}\chi) = 0, \tag{12}$$

$$(1 + \varepsilon\theta)\theta'' + \text{Rd}(1 + (\theta_w - 1)\theta)^2(3(\theta_w - 1)\theta'^2 + \theta''(1 + (\theta_w - 1)\theta)) + \varepsilon(\theta')^2 + \text{Pr}[\text{Nb}\theta'\phi' + f\theta' + \text{Nt}\theta'^2 + Q\theta] = 0, \tag{13}$$

$$\phi'' + \left(\frac{\text{Nt}}{\text{Nb}}\right)\theta'' + \text{Le}\,\text{Pr}\,f\phi' - \text{Le}\,\text{Pr}\,\sigma(1 + \delta\theta)^n\phi\exp\left(-\frac{E}{1 + \delta\theta}\right) = 0, \tag{14}$$

$$\chi'' + \text{Lb}f\chi' - \text{Pe}(\phi''(\chi + \delta_1) + \chi'\phi') = 0. \tag{15}$$

The boundary conditions in non-dimensional form are as follows:

$$\left.\begin{aligned} &f(0)=0, \quad f'(0)=1+\alpha f''(0)+\beta f'''(0),\\ &\theta'(0)=\mathrm{Bi}(\theta(0)-1), \quad \mathrm{Nb}\theta'(0)+\mathrm{Nt}\varphi'(0)=0, \quad \chi(0)=1,\\ &f'(\infty)\to 0, \quad \theta(\infty)\to 0, \quad \varphi(\infty)\to 0, \quad \chi(\infty)\to 0, \end{aligned}\right\} \tag{16}$$

where couple stress fluid parameter is K, Hartmann number symbolized by M, buoyancy ratio parameter is Nr, bioconvection Rayleigh number denoted by Nc, mixed convection parameter is λ, Prandtl number denoted by Pr, heat source sink parameter is Q, variable thermal conductivity constant expressed by ε, thermophoresis parameter is Nt, Nb the Brownian motion parameter, Rd for thermal radiation parameter, temperature ratio parameter θ_w, Lewis number Le, reaction constant σ^{**}, activation energy constant E, temperature difference parameter δ, Peclet number Pe, Lb for bioconvection Lewis number, δ_1 the microorganism concentration difference constant, thermal Biot number is denoted by Bi, first-order slip is α and second-order slip constants β are defined as follows:

$$K=\eta^* c/\rho\nu^2, \quad M=\frac{\sigma^* B_0^2}{\rho_f c}, \quad \mathrm{Nr}=\frac{(\rho_p-\rho_f)(C_w-C_\infty)}{\beta\rho_f(1-C_\infty)T_\infty},$$

$$\mathrm{Nc}=\frac{\gamma(\rho_m-\rho_f)(n_w-n_\infty)}{\beta\rho_f(1-C_\infty)T_\infty}, \quad \lambda=\left(\frac{(T_\infty)\beta_1 g_1(1-C_\infty)}{c(\rho c)_f}\right), \quad \mathrm{Pr}=\frac{\nu}{\alpha_e},$$

$$Q=Q_0/c(\rho c_p)_f, \quad \mathrm{Nt}=\frac{(\rho c_p)_p D_B(T_f-T_\infty)}{T_\infty\nu(\rho c_p)_f}, \quad \mathrm{Nb}=\frac{(\rho c_p)_p D_B C_\infty}{(\rho c_p)_f\nu},$$

$$\mathrm{Rd}=\frac{16\sigma^{**}T_\infty^3}{3k^*k}, \quad \theta_w=\frac{T_w}{T_\infty}, \quad \mathrm{Le}=\frac{\alpha}{D_B}, \quad \sigma=\frac{k_a}{c}, \quad E=\frac{E_a}{K_1 r T_\infty},$$

$$\delta=\frac{T_w-T_\infty}{T_\infty}, \quad \mathrm{Pe}=\frac{bW_c}{D_m}, \quad \mathrm{Lb}=\frac{\nu}{D_m}, \quad \mathrm{Pe}=\frac{bw_c}{D_m},$$

$$\delta_1=\frac{n_\infty}{n_w-n_\infty}\mathrm{Bi}=(h_f/k)\sqrt{\nu/c}, \quad \alpha=A\sqrt{\frac{c}{\nu}}, \quad \beta=\frac{Gc}{\nu}.$$

The dimensionless forms of skin friction coefficient, local Nusselt number, local Sherwood number and motile density number are given below

$$\mathrm{Re}_x^{1/2}\, C_f = f''(0)-Kf''''(0), \tag{17}$$

$$\mathrm{Re}_x^{-1/2}\, \mathrm{Nu}_x = -\theta'(0), \tag{18}$$

$$\mathrm{Re}_x^{-1/2}\, \mathrm{Sh}_x = -\varphi'(0), \tag{19}$$

$$\mathrm{Re}_x^{-1/2} N_n = -\chi'(0). \tag{20}$$

3. Numerical Scheme

The dimensionless ordinary differential equations (12)–(15) with relative boundary constraints (16) are highly nonlinear in behavior. The shooting scheme is adapted

for handling these nonlinear systems of ODE's. The outcomes of ordinary differential equations are obtained by competent bvp4c built-in function MATLAB, one of the collection schemes which utilize the Lobatto-IIIa formula. The shooting technique is more flexible and the initial guesses control the convergence criteria. The higher order ordinary differential equations are reduced to first-order boundary values problem by introducing some new variables.

Let

$$\begin{aligned} f = q_1, \quad f' = q_2, \quad f'' = q_3, \quad f''' = q_4, \\ f^{iv} = q_5, \quad f^v = q_5', \quad \theta = q_6, \quad \theta' = q_7, \\ \theta'' = q_7', \quad \phi = q_8, \quad \phi' = q_9, \quad \phi'' = q_9', \\ \chi = q_{10}, \quad \chi' = q_{11}, \quad \chi'' = q_{11}', \end{aligned} \tag{21}$$

$$q_5' = \frac{(1-(\gamma q_6))q_4 - \gamma q_7 q_3 - q_2^2 + q_1 q_3 - M q_2 + \lambda(q_6 - \mathrm{Nr} q_8 - \mathrm{Nc} q_{10})}{K}, \tag{22}$$

$$q_7' = \frac{\begin{array}{c} -\mathrm{Rd}(1+(\theta_w-1)q_6)^2(3(\theta_w-1)q_7^2) - \varepsilon q_7^2 \\ -\mathrm{Pr}[\mathrm{Nb} q_7 q_9 + q_1 q_7 + \mathrm{Nt} q_7^2 + Q q_6] \end{array}}{(1+\varepsilon q_6) + \mathrm{Rd}(1+(\theta_w-1)q_6)^3}, \tag{23}$$

$$q_9' = -\left(\frac{\mathrm{Nt}}{\mathrm{Nb}}\right) q_7' - \mathrm{Le}\,\mathrm{Pr}\, q_1 q_9 + \mathrm{Le}\,\mathrm{Pr}\,\sigma(1+\delta q_6)^n q_8 \exp\left(-\frac{E}{1+\delta q_6}\right), \tag{24}$$

$$\chi'' = -\mathrm{Lb} q_1 q_{11} + \mathrm{Pe}(q_9'(q_{10}+\delta_1) + q_{11} q_9). \tag{25}$$

With

$$\left.\begin{array}{l} q_1(0) = 0, \quad q_2(0) = 1 + \alpha q_3(0) + \beta q_4(0), \\ q_7(0) = \mathrm{Bi}(q_6(0) - 1), \quad \mathrm{Nb} q_7(0) + \mathrm{Nt} q_9(0) = 0, \quad q_{10}(0) = 1, \\ q_2(\infty) \to 0, \quad q_6(\infty) \to 0, \quad q_8(\infty) \to 0, \quad q_{10}(\infty) \to 0. \end{array}\right\} \tag{26}$$

4. Results and Discussion

The consequence of pertinent dimensionless parameter on flow fields, namely, velocity, temperature, and concentration of nanoparticles and microorganisms profile are highlighted graphically in this slice. Figures 1–15 are captured to estimate the physical behavior of prominent parameters.

Figure 1 is designed to examine the consequences of first-order velocity slip parameter α and magnetic parameter M via velocity of fluid f'. It is analyzed that velocity f' is reduced by growing values of first-order velocity slip parameter α and magnetic parameter M. The roles of buoyancy ratio parameter Nr and second-order velocity slip parameter β on velocity f' are visualized in Fig. 2. For variations of buoyancy ratio parameter Nr and second-order velocity slip parameter β, the flow of fluid f' declines. Figure 3 is captured to examine the impact of couple stress fluid parameter K and mixed convection parameter λ via flow profile f'.

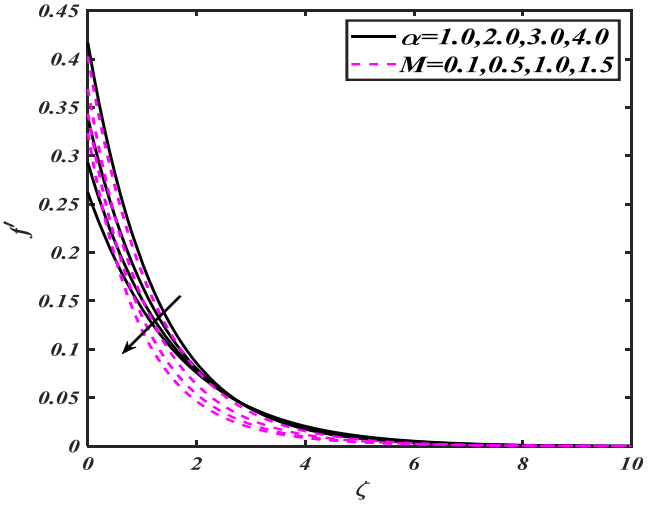

Fig. 1. (Color online) f' versus α and M.

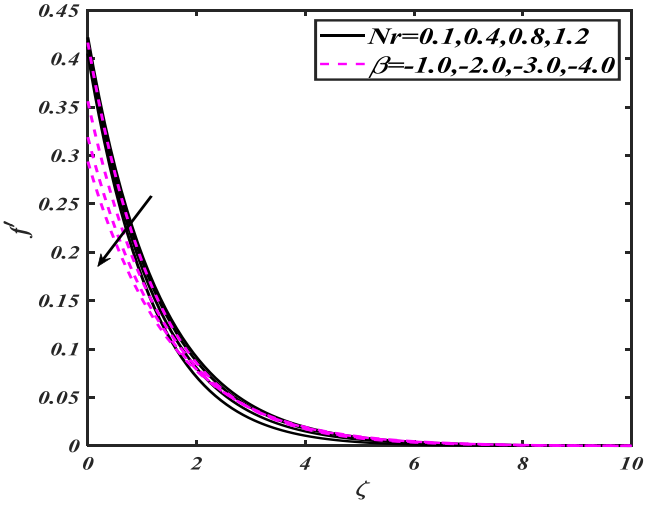

Fig. 2. (Color online) f' versus Nr and β.

The effect of Prandtl number Pr and thermal conductivity parameter ε against temperature distribution θ is displayed in Fig. 4. The growing thermal conductivity parameter ε escalates the temperature distribution θ while Prandtl number Pr has reverse impact. Figure 5 manifests the impact of thermophoresis parameter Nt and Radiation parameter Rd against the temperature field θ curves. It is remarked that temperature distribution θ increases with the increment of thermophoresis parameter Nt. From the temperature curves, it also depicted that temperature distribution θ is enhanced by escalating the values of radiation parameter Rd. The

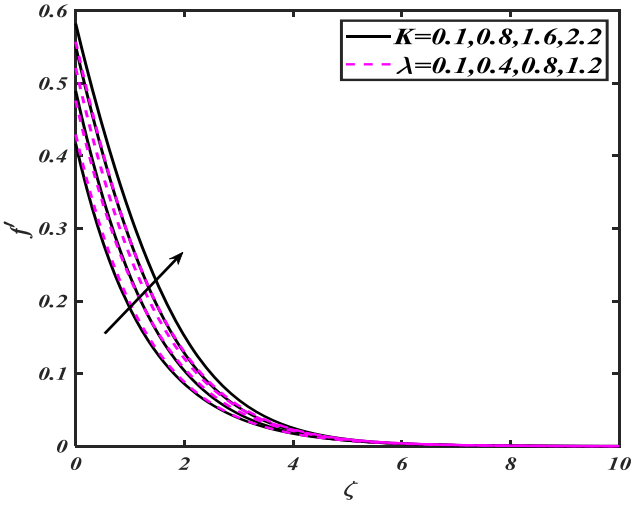

Fig. 3. (Color online) f' versus K and λ.

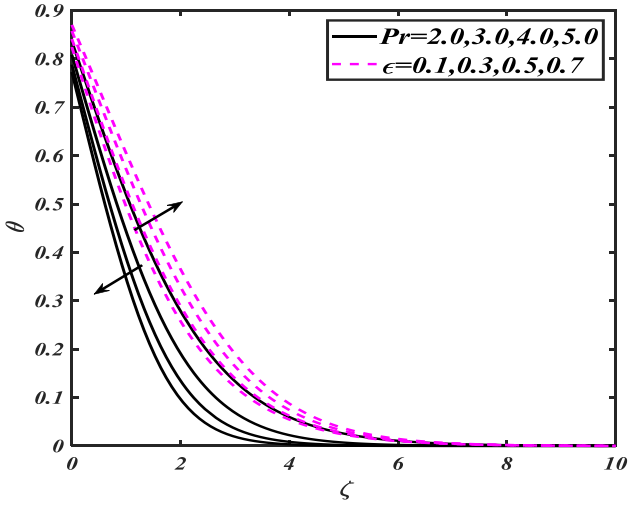

Fig. 4. (Color online) θ versus Pr and ε.

estimations of temperature field θ for various magnitudes of Biot number Bi and heat generation/observation parameter Q is shown in Fig. 6. Larger values of both values of these parameters enhanced the temperature distribution θ. Characteristics of first-order velocity slip parameter α and buoyancy ratio parameter Nr against temperature field θ are discussed in Fig. 7. Here temperature profile enhances when buoyancy ratio parameter Nr and first-order velocity slip parameter α are escalated. Salient features of couple stress fluid parameter K and mixed convection parameter λ via temperature profile θ are seen in Fig. 8. From this picture, it is examined that

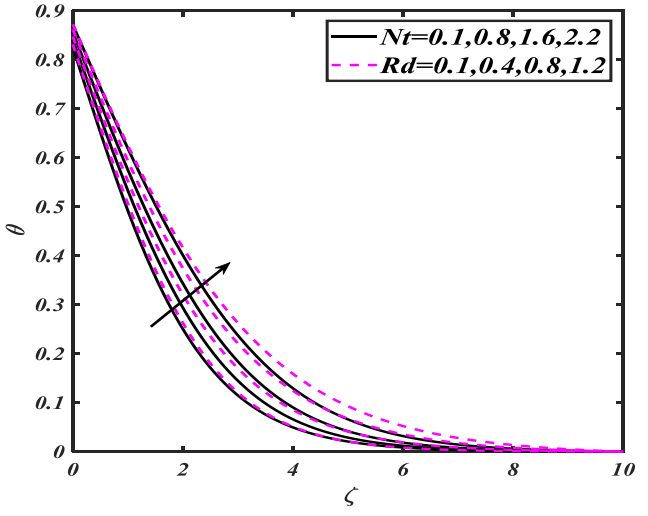

Fig. 5. (Color online) θ versus Nt and Rd.

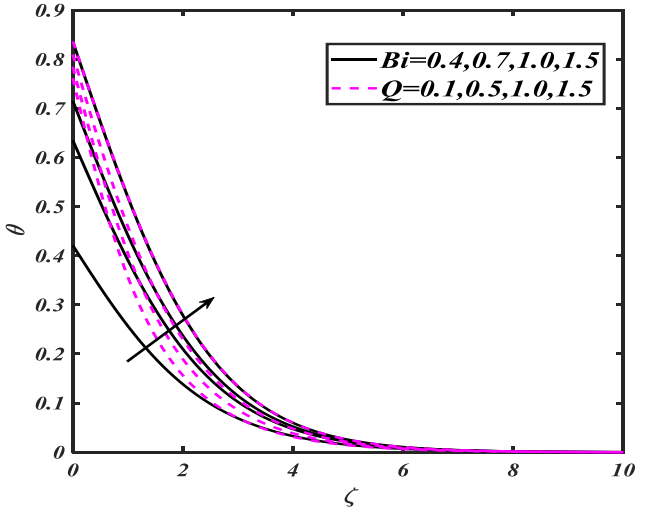

Fig. 6. (Color online) θ versus Bi and Q.

thermal distribution θ declined for larger estimation of couple stress fluid parameter K and mixed convection parameter λ.

Figure 9 is captured to examine the change in concentration of nanoparticles ϕ for greater amount of thermophoresis parameter Nt and Brownian motion parameter Nb. It is scrutinized that concentration field of nanoparticles ϕ diminishes with an augmentation in Brownian motion parameter Nb while inverse behavior is depicted for thermophoresis parameter Nt. Physically, thermal conductivity rises

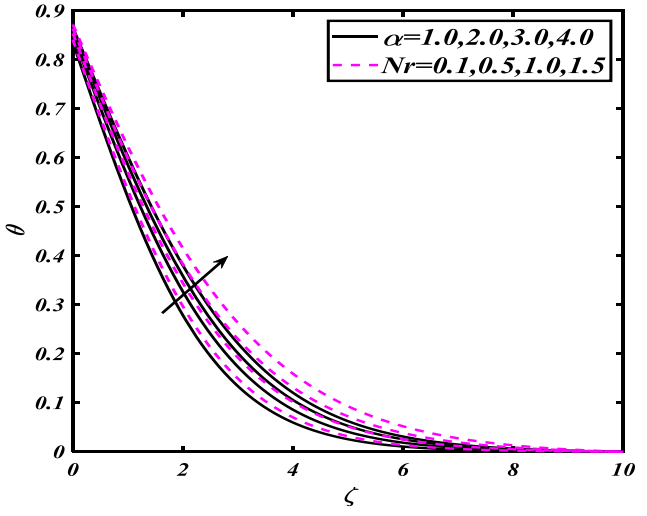

Fig. 7. (Color online) θ versus α and Nr.

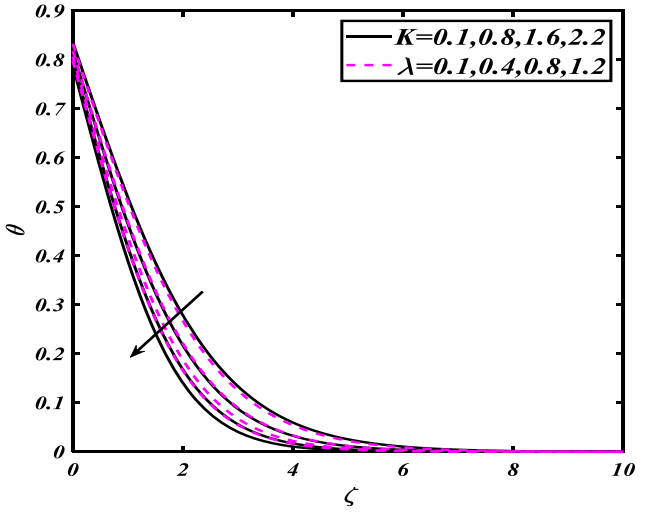

Fig. 8. (Color online) θ versus K and λ.

for larger thermophoresis parameter. In thermophoresis mechanisms, the nanoparticles of the fluid are dragged back from the hot to cold region. Thus, the fluid particles moved back from the surface, which is heated and consequently concentration increases. Owing to larger thermal conductivity, convection rises.

Figure 10 depicts behavior of temperature distribution θ for distinguished variations of Lewis number Le and activation energy parameter E. The upsurge in Lewis number Le diminishes the temperature distribution θ while it increased for

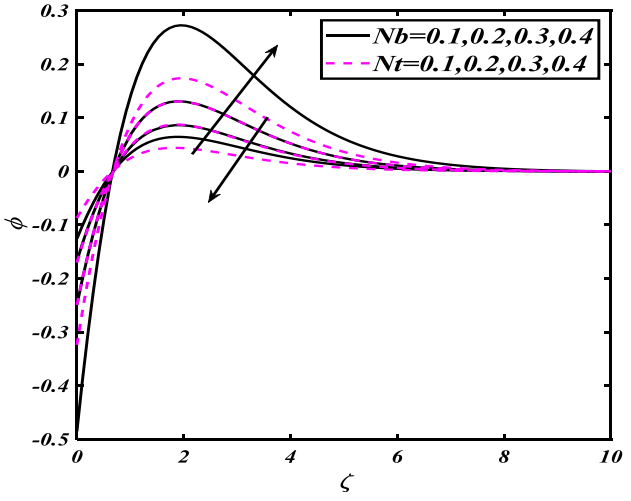

Fig. 9. (Color online) ϕ versus Nb and Nt.

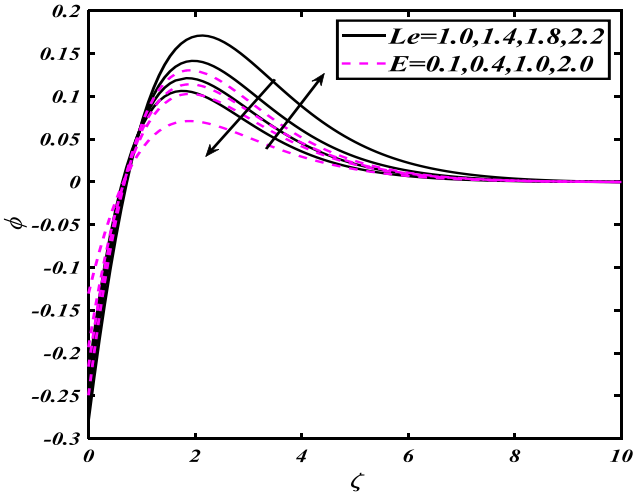

Fig. 10. (Color online) ϕ versus Le and E.

larger amount of activation energy parameter E. Figure 11 is designed to illustrate the effect of first-order velocity slip parameter α and buoyancy ratio parameter Nr against concentration of nanomaterials ϕ. Clearly, concentration ϕ is boosted up by growing the values of first-order velocity slip parameter α and buoyancy ratio parameter Nr. Figure 12 reveals the impact of couple stress fluid parameter K and mixed convection parameter λ on solutal field of species ϕ. It is noted that concentration of species ϕ decays with an enhancement in couple stress fluid parameter K and mixed convection parameter λ.

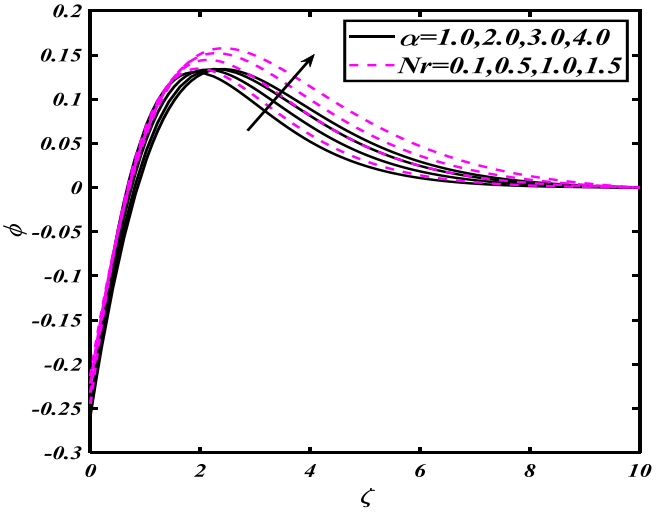

Fig. 11. (Color online) ϕ versus α and Nr.

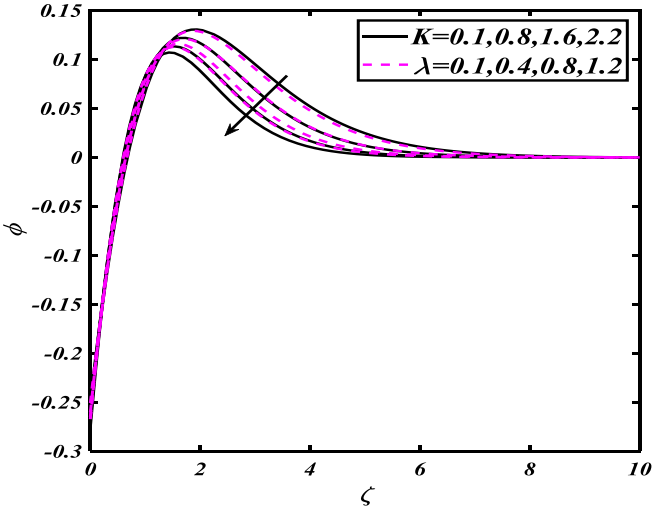

Fig. 12. (Color online) ϕ versus K and λ.

The curves of microorganisms profile χ for the effects of Peclet number Pe and bioconvection Lewis number Lb are elaborated in Fig. 13. It is observed that concentration of microorganisms χ boosted up under the action of Peclet number Pe and bioconvection Lewis number Lb. Figure 14 reveals the consequence of couple stress fluid parameter K and mixed convection parameter λ on concentration of microorganisms χ. From this figure, it is witnessed that concentration of microorganisms χ dwindles for higher couple stress fluid parameter K and mixed convection

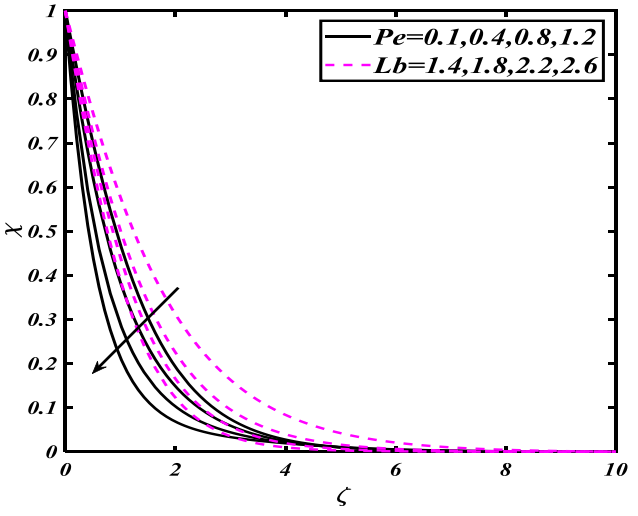

Fig. 13. (Color online) χ versus Pe and Lb.

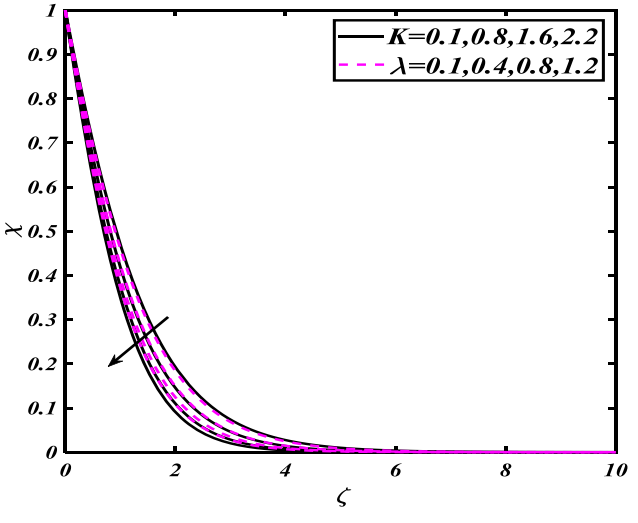

Fig. 14. (Color online) χ versus K and λ.

parameter λ. Figure 15 indicates the behavior of first-order velocity slip parameter α and bioconvection Rayleigh number Nc on concentration of microorganisms χ. It is noted that concentration of microorganism χ rises against higher amount of first-order velocity slip parameter α and bioconvection Rayleigh number Nc.

In this slice numerical outcomes are discussed through tabular data. The numerical result of local skin friction coefficient is presented in Table 1. It is analyzed that skin friction coefficient $-f''(0)$ boosted up for higher estimation of magnetic

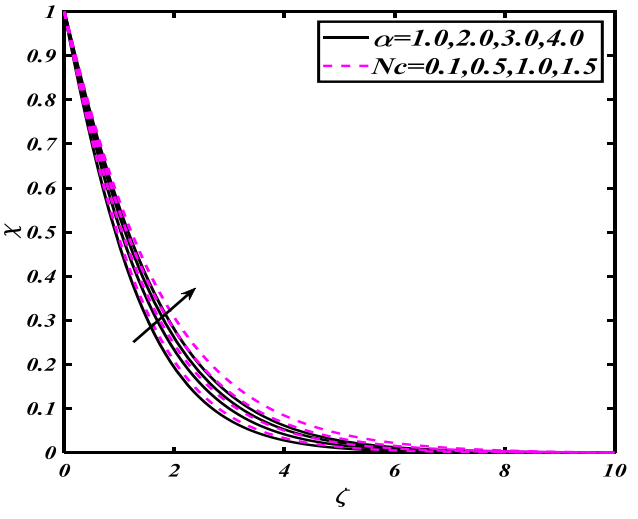

Fig. 15. (Color online) χ versus α and Nc.

Table 1. Variation of skin friction coefficient for distinguished magnitudes of emerging parameters.

M	K	λ	Nr	Nc	α	β	$-f''(0)$
0.2	0.5	0.1	0.1	0.5	1.0	−1.0	0.3196
0.6							0.3231
1.0							0.3245
0.5	0.2						0.3215
	0.6						0.3228
	1.0						0.3240
		0.2					0.3152
		0.4					0.3068
		0.8					0.2995
			0.2				0.3231
			0.6				0.3256
			1.0				0.3283
				0.2			0.3225
				1.0			0.3229
				2.0			0.3283
					2.0		0.2396
					3.0		0.1906
					4.0		0.1583
						−2.0	0.2470
						−3.0	0.2016
						−4.0	0.1711

Table 2. Variation of local Nusselt number of coefficient for distinguished variation of various parameters.

M	K	λ	Nr	Nc	α	β	Pr	Nt	Bi	Q	Rd	$-\theta'(0)$
0.2	0.5	0.1	0.1	0.5	1.0	−1.0	2.0	0.3	2.0	0.2	0.8	0.2834
0.6												0.2518
1.0												0.2284
0.5	0.2											0.2572
	0.6											0.2594
	1.0											0.2616
		0.2										0.2795
		0.4										0.3069
		0.8										0.3408
			0.2									0.2589
			0.6									0.2589
			1.0									0.2494
				0.2								0.2640
				1.0								0.2489
				2.0								0.2174
					2.0							0.2359
					3.0							0.2217
					4.0							0.2120
						−2.0						0.2380
						−3.0						0.2249
						−4.0						0.2159
							2.5					0.2847
							3.0					0.3070
							3.5					0.3263
								0.1				0.2697
								0.4				0.2535
								0.8				0.2331
									3.0			0.2705
									4.0			0.2767
									5.0			0.2806
										0.1		0.2582
										0.3		0.2595
										0.6		0.2615
											1.0	0.2486
											1.5	0.2279
											2.0	0.2121

parameter M, buoyancy ratio parameter Nr and bioconvection Rayleigh number Nc. From Table 2, it is depicted that local Nusselt number $-\theta'(0)$ reduces for larger radiation parameter Rd and magnetic parameter M. The local Sherwood number $\phi'(0)$ enlarged for higher Prandtl number Pr while decreases with thermophoresis parameter Nt, which is displayed in Table 3. From Table 4, it is noted that local density number of microorganisms $-\chi'(0)$ enhanced for larger variation of Peclet number Pe and bioconvection Lewis number Lb.

Table 3. Variation of local Sherwood number of coefficient for distinguished magnitudes of emerging parameters.

M	K	λ	Nr	Nc	α	β	Pr	Nt	Nb	Le	$\phi'(0)$
0.2	0.5	0.1	0.1	0.5	1.0	−1.0	2.0	0.3	0.2	2.0	0.4251
0.6											0.3778
1.0											0.3426
0.5	0.2										0.3858
	0.6										0.3891
	1.0										0.3925
		0.2									0.4192
		0.4									0.4604
		0.8									0.5113
			0.2								0.3869
			0.6								0.3808
			1.0								0.3741
				0.2							0.3961
				1.0							0.3733
				2.0							0.3261
					2.0						0.353
					3.0						0.3325
					4.0						0.3181
						−2.0					0.3570
						−3.0					0.3374
						−4.0					0.3239
							2.5				0.4271
							3.0				0.4604
							3.5				0.4894
								0.1			0.1348
								0.4			0.5071
								0.8			0.9322
									0.1		0.3545
									0.4		0.3324
									0.8		0.3122
										3.0	0.3860
										4.0	0.3845
										5.0	0.3834

Table 4. Variation of local microorganism's density number of coefficient for distinguished variations of emerging parameters.

M	K	λ	Nr	Nc	α	β	Pe	Lb	$-\chi'(0)$
0.2	0.5	0.1	0.1	0.5	1.0	−1.0	0.1	2.0	0.6519
0.6									0.5811
1.0									0.5275
0.5	0.2								0.5929
	0.6								0.5984
	1.0								0.6039
		0.2							0.6410
		0.4							0.7015
		0.8							0.7794
			0.2						0.5952
			0.6						0.5874
			1.0						0.5788
				0.2					0.6091
				1.0					0.5737
				2.0					0.5009
					2.0				0.5363
					3.0				0.4981
					4.0				0.4719
						−2.0			0.5419
						−3.0			0.5068
						−4.0			0.4824
							0.5		0.8867
							1.5		1.6501
							2.0		2.0476
								2.5	0.6994
								3.0	0.7931
								3.5	0.8802

5. Conclusions

Here the feature of thermal-dependent conductivity in nonlinear radiative flow of couple stress fluid including small solid particles and motile microorganism is investigated. The mechanism of bioconvection is scrutinized in couple stress fluid. The effect of distinguished influential parameters against velocity, thermal field, concentration of nanoparticles and concentration of microorganism are disclosed. The major outcomes are listed below:

- A lower velocity profile is perceived with escalating second-order velocity slip parameter and magnetic parameter.
- Larger couple stress parameter, enhanced the velocity field.
- Velocity of fluid reduces for larger magnitudes of bioconvection Rayleigh number.
- Temperature grows for higher thermal-dependent conductivity, thermophoresis parameter and temperature ratio parameter.

- Impact of Prandtl number and Lewis number via concentration field of species are similar.
- Activation energy improves the concentration field of species.
- An enhancement in the magnitudes of Peclet number and bioconvection Lewis number caused diminution in concentration of motile microorganisms.
- The concentration of microorganisms increases by escalating the amount of first-order velocity slip parameter and bioconvection Rayleigh number.

Acknowledgment

The authors extend their appreciation to the Deanship of Scientific Research at King Khalid University, Abha 61413, Saudi Arabia for funding this work through research groups program under grant number R.G.P-1/234/42.

References

1. S. U. S. Choi and J. A. Eastman, Enhancing thermal conductivity of fluids with nanoparticles, in *Proc. 1995 ASME Int. Mechanical Engineering Congress and Exposition*, San Francisco, CA (1995).
2. J. Buongiorno, *J. Heat Transfer* **128**, 240 (2006).
3. I. Waini, A. Ishak and I. Pop, *Alexandria Eng. J.* **59**, 91 (2020).
4. L. A. Lund *et al.*, *Symmetry* **12**, 276 (2020).
5. B. Kumar and S. Srinivas, *J. Appl. Comput. Mech.* **6**, 259 (2020).
6. S. Abdal *et al.*, *Symmetry* **12**, 49 (2020).
7. B. Gireesha *J. Phys. A, Stat. Mech. Appl.* 124051 (2020).
8. M. R. Khan *et al.*, *Int. Commun. Heat Mass Transf.* **116**, 104707 (2020).
9. T. Hayat *et al.*, *Int. Commun. Heat Mass Transf.* **111**, 104445 (2020).
10. S. A. Khan, Y. Nie and B. Ali, *SN Appl. Sci.* **2**, 66 (2020).
11. B. Ali *et al.*, *Powder Technol.* (2020).
12. S. U. Khan *et al.*, *Phys. Scr.* **94**, 125211 (2019).
13. M. I. Khan, *Int. Commun. Heat Mass Transf.* **122**, 105177 (2021).
14. H. Waqas *et al.*, *Appl. Math. Mech.* **40**, 1255 (2019).
15. S. U. Khan *et al.*, *J. Thermal Anal. Calorim.* **143**, 1175 (2021).
16. N. Sadiq *et al.*, *J. Appl. Environ. Biol. Sci.* **8**, 157 (2018).
17. A. R. Bestman, *Int. J. Energy Res.* **14**, 389 (1990).
18. M. Waqas *et al.*, *Int. Commun. Heat Mass Transf.* **112**, 104401 (2020).
19. T. Hayat *et al.*, *Phys. A, Stat. Mech. Appl.* **549**, 124006 (2020).
20. G. Sandhya *et al.*, *Heat Transf.* **50** (2020), doi:10.1002/htj.21904.
21. M. I. Khan, *Chin. J. Chem. Eng.* **31**, 17 (2021).
22. M. Z. Ullah *et al.*, *Phys. A, Stat. Mech. Appl.* **550**, 124024 (2020).
23. N. S. Khan, P. Kumam and P. Thounthong, *Sci. Rep.* **10**, 1 (2020).
24. S. Naz *et al.*, *Appl. Nanosci.* **10**, 3183 (2020).
25. M. I. Khan *et al.*, *J. Mater. Res. Technol.* **9**, 9951 (2020).
26. J. R. Platt, *Science* **133**, 1766 (1961), http://dx.doi.org/10.1126/science.133.3466.1766.
27. M. N. Khan and S. Nadeem, *Can. J. Phys.* **98**, 732 (2020).
28. S. K. Mondal and D. Pal, *J. Comput. Design Eng.* **7**, 251 (2020).

29. F. Ayodeji, A. Tope and O. Pele, *Mach. Learn. Res.* **4**, 51 (2020).
30. M. I. Khan *et al.*, *Phys. Scr.* **96**, 055005 (2021).
31. M. Ferdows *et al.*, *Symmetry* **12**, 692 (2020).
32. M. I. Khan *Mod. Phys. Lett. B* **35**, 2150202 (2021).
33. M. F. M. Basir, *Chin. J. Phys.* **65**, 538 (2020).
34. V. M. Magagula, S. Shaw and R. R. Kairi, *Heat Transf.* **49** (2020), doi:10.1002/htj.21730.